IEEE Access
Multidisciplinary | Rapid Review | Open Access Journal

Received March 6, 2019, accepted March 19, 2019, date of publication March 29, 2019, date of current version April 17, 2019.

*Digital Object Identifier 10.1109/ACCESS.2019.2908232*

# An Object-Based River Extraction Method via Optimized Transductive Support Vector Machine for Multi-Spectral Remote-Sensing Images

**XIN LI[1], (Member, IEEE), XIN LYU[1], YAO TONG[2], SHENGYANG LI[3], AND DAOFANG LIU[3]**

[1]College of Computer and Information, Hohai University, Nanjing 210000, China
[2]Industrial Technology Research Institute, Zhengzhou University, Zhengzhou 450000, China
[3]Information Center, Yellow River Conservancy Commission, Zhengzhou 450000, China

Corresponding author: Xin Lyu (lvxin@ hhu.edu.cn)

This work was supported in part by the National Key Research and Development Program of China under Grant 2018YFC0407105, in part by the General Program of the National Natural Science Foundation of China under Grant 61272543, in part by the NSF-China and Guangdong Province Joint Project under Grant U1301252, in part by the Fundamental Research Funds for the Central Universities under Grant 2019B64314, and in part by the Postgraduate Research and Practice Innovation Program of Jiangsu Province under Grant SJKY19_0446.

**ABSTRACT** The accurate extraction of rivers is closely related to agriculture, socio-economic, environment, and ecology. It helps us to pre-warn serious natural disasters such as floods, which leads to massive losses of life and property. With the development and popularization of remote-sensing and information technologies, a great number of river-extraction methods have been proposed. However, most of them are vulnerable to noise interference and perform inefficient in a big data environment. To address these problems, a river extraction method is proposed based on adaptive mutation particle swarm optimization (PSO) support vector machine (AMPSO-SVM). First, three features, the spectral information, normalized difference water index (NDWI), and spatial texture entropy, are considered in feature space construction. It makes the objects with the same spectrum more distinguishable, then the noise interference could be resisted effectively. Second, in order to address the problems of premature convergence and inefficient iteration, a mutation operator is introduced to the PSO algorithm. This processing makes transductive SVM obtain optimal parameters quickly and effectively. The experiments are conducted on GaoFen-1 multispectral remote-sensing images from Yellow River. The results show that the proposed method performs better than the existed ones, including PCA, KNN, basic SVM, and PSO-SVM, in terms of overall accuracy and the kappa coefficient. Besides, the proposed method achieves convergence rate faster than the PSO-SVM method.

**INDEX TERMS** River extraction, particle swarm optimization, SVM, GaoFen-1 remote-sensing image.

## I. INTRODUCTION

Inland waters such as lakes, rivers and reservoirs play key roles in regional biogeochemical cycles [1]. It is necessary to accurately evaluate the area and shape of water bodies [2], [3]. Changes in river status impact irrigation, energy production, fishery and transportation [4], [5], and rivers in urban areas may cause surface subsidence, urban inland inundation and water-related disease epidemics [6]. Therefore, it is necessary to monitor and evaluate the distribution and river conditions.

In recent years, satellite remote-sensing technology has been developing rapidly, with a wide swath and a short return period [7]. It has been widely applied in many fields, such as military reconnaissance, environmental protection and agriculture [8]–[11].

The remote-sensing image has massive spatial information besides spectral information than before. It poses a substantial challenge in the field of remote-sensing image processing. Most high-resolution remote-sensing images only have four bands (blue, green, red, and near-infrared). They lack necessary spectral information to computing the modified normalized difference water index (MNDWI) [12] and automated water extraction index (AWEI) [13].

Conventional spectrum-based classification methods consider an image as an ensemble of spectral measurements, while neglecting the spatial organization of pixels [14]–[17];

The associate editor coordinating the review of this manuscript and approving it for publication was Mehul S. Raval.

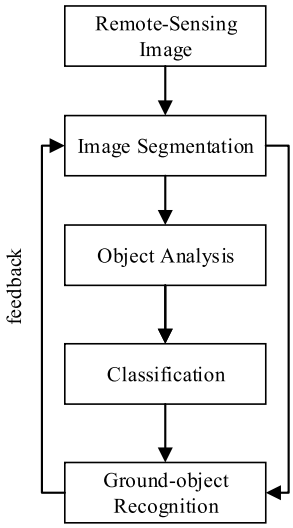


**FIGURE 1.** OBIA of a remote-sensing image.

Shao *et al.* [18] analyzed traditional methods and indicated that the existing methods cannot effectively avoid "different bodies with the same spectrum" and "same body with different spectra" phenomenon. Castilla [19] proposed an object-based method to address the problems above-mentioned in landscape mapping and extended it to the field of image analysis. Blaschke *et al.* [20] firstly summarized characteristics of the object-based method in image analysis and named it as object-based image analysis (OBIA), which is the definition that most scholars now use. For remote-sensing image processing, the OBIA process is illustrated in Fig. 1. Moreover, Ganim and Tokmakoff [21] demonstrated the feasibility and effectiveness of object-based methods in details. Since that, many object-based remote sensing processing methods have been developed. In [22], an object-based extraction method was proposed and applied to high-resolution remote-sensing images by considering the hierarchical spectrum and shape features; an accuracy rate of 94.6% was realized. In [23], an object-based workflow was formed that focuses on shallow-water aquatic vegetation in multispectral imagery. Additionally, Selmes *et al.* [24] applied an object-based segmentation method to extract lakes and the error was within 0.125 $km^2$; however, the method didn't perform well on river extraction because of the uncertainty regarding the boundary. In [25], a multiresolution segmentation method was proposed for extracting buildings from very high resolution imagery with high accuracy. Li *et al.* [26] improved the watershed segmentation algorithm and obtained clear boundaries of water and vegetation areas based on OBIA. In [27], an object-based water classification extraction model was proposed that combined MXL and the ISODATA algorithm and yielded satisfactory accuracy. In [8], an image sharpening approach was conducted on Sentinel-2A multispectral instrument imagery (MSI) for mapping water bodies. To sum up, the object-based methods outperformed the traditional pixel-based method on remote-sensing image classification and extraction [28]. Specifically, the object-based methods that consider other features besides spectral information, such as KNN method, PCA method and SVM-based method, achieve the reduction of wrong extraction and classification results.

With further exploration of the application of computer technology, the support vector machine (SVM) [29] has been applied to remote-sensing image processing. In [30], SVM is utilized to construct a multispectral remote-sensing land use classification model and compared with the maximum likelihood method and decision tree method, which further demonstrated the advantages of SVM in terms of accuracy and stability. Chen *et al.* [31] proposed a multilevel stacking SVM improved classification model for effectively distinguishing the information of two feature spaces and maintaining strong generalization ability while realizing higher classification accuracy for remote-sensing images. Guo *et al.* [32] proposed an SVM-based sequential classifier training approach, which uses the previous images to reduce the number of samples to enhance the performance of SVM; this model outperformed state-of-the-art algorithms on multitemporal remote-sensing images. Moreover, an improved SVM which using particle swarm optimization algorithm has been proposed and applied to land cover classification [33]. According to this method, the SVM parameters' optimization is meaningful for the whole results of SVM-based method. Reference [34] developed an alternative extraction method for urban area by utilizing VIIRS DNB and MODIS NDVI data. This article incorporating mutation particle swarm optimization and SVM theories and achieves high classification coherency with Landsat8 OLI results.

In general, the SVM algorithm performs stably and accurately when applied to information extraction from remote-sensing image. However, it is necessary to carry out intensive research on precisely extracting a river via SVM with higher accuracy and efficiency. Motivated by this point, we develop an improved support vector machine method. In this method, we build an AMPSO-SVM-based river extraction framework combined with the feature space we constructed, in which the spectral and texture features and water index are considered in the feature space. In addition, the particle swarm optimization algorithm with a mutation operator (AMPSO, Adaptive Mutation Particle Swarm Optimization) is presented to avoid the premature convergence phenomenon and lift up the iteration efficiency during the training process of the SVM classifier. In the experiments, the proposed method is compared with the PCA method [35], the KNN method [36], an SVM-based method and a PSO-SVM-based method.

The main contributions of this study are summarized as follows:

1) A novel object-based river extraction method via AMPSO-SVM is presented. First of all, the feature space is expanded by spectral information, NDWI and texture entropy. Besides, a mutation particle swarm optimization algorithm is introduced to help transductive SVM avoid premature convergence and increase iteration efficiency.

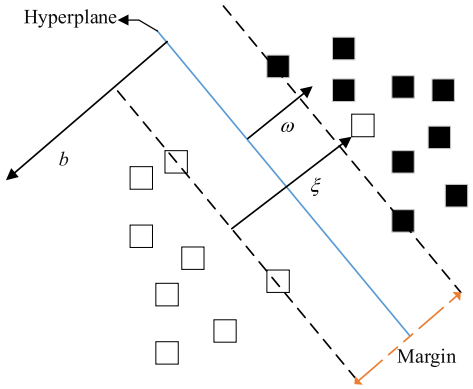


**FIGURE 2.** Basic SVM.

2) To evaluate the performance of the proposed method, an object-based river extraction framework is integrated by feature space construction module, AMPSO-SVM classifier and automated river extraction module. Making full use of the spatial feature, spectral feature of objects and the stability and efficiency of AMSO-SVM classifier, then we successfully extracts river water bodies from multi-spectral remote-sensing images with higher accuracy and less iterations by proposed method.

The remainder of this paper is organized as follows: In Section 2, preliminaries are introduced. Section 3 briefly introduces the proposed method. The experimental results on the real data sets are presented in Section 4. The conclusions of this study and future work are discussed in Section 5.

## II. PRELIMINARIES

### A. BASIC SVM THEORY

Support vector machine (SVM) has substantial potential in the classification of remotely sensed data. As a machine learning algorithm, SVM is a supervised classification algorithm. Given a training sample and the category to which it belongs, the classification model is calculated from the sample via an algorithm and extended to the item to be classified. Finally, the category to which this item belongs is obtained according to the value of the discriminant function. With a simple structure and strong generalization ability, SVM performs well on problems that have high-dimensional features and uncertainties [37]. SVM is a very attractive approach for the classification of remotely sensed data. This approach seeks to find the optimal separating hyperplane between classes by focusing on the training cases that lie at the edges of the class distributions, namely, the support vectors. The main parameters of SVM are penalty parameters and kernel function parameters. The former control the punishment severity for the incorrect classification of a sample. In general, the larger the value of c is, the smaller the maximum spacing between two hyperplanes is, the smaller the number of misclassified samples is, and the longer the training time is.

As shown in Fig. 2, classification via SVM can be illustrated easily for the simple situation in which there are two linearly separable classes in q-dimensional space. Using the training data, which are represented by $\{x_i, y_i\}, i = 1, \ldots, r, y_i \in \{1, -1\}$, many hyperplanes could be fitted to separate the classes; however, there is only one optimal separating hyperplane, which is expected to generalize well in comparison to other hyperplanes. This optimal hyperplane should run between the two classes, with all cases of a class located on the same side of the separating hyperplane, such that the distance from the hyperplane to the closest training data points in both classes is as large as possible.

A hyperplane can be defined by the equation $\omega \cdot x_i + b = 0$, where $x$ is a point that lies on the hyperplane, $\omega$ is normal to the hyperplane,$b$ is the bias, and $(b)/(\|\omega\|)$ is the perpendicular distance from the hyperplane to the origin. For the linear partitioning problem, a hyperplane can be defined as $y_i(\omega \cdot x_i + b) - 1 \geq 0$.

### B. TRANSDUCTIVE SVM

In this part, we adopt transductive support vector machine (TSVM) as the initial SVM classifier, which is a classifier for binary classification problems. Similar to traditional SVM, TSVM searches for a hyperplane that has the largest margin and separates the classes; it takes into account both labeled and unlabeled examples.

Formally, a set of labeled examples can be denoted as $D_l = \{(x_1, y_1), (x_2, y_2), \ldots, (x_i, y_i)\}$ and a set of unlabeled examples as $D_u = \{x_{l+1}, x_{l+2}, \ldots, x_{l+u}\}$, where $y_i \in \{+1, -1\}$, $l \gg u$, $l + u = m$. We aim at predicting and labeling the samples from $D_u : \hat{y} = (y_{l+1}, y_{l+2}, \ldots, y_{l+u}), \hat{y} \in (+1, -1)$. The learning process of TSVM can be formulated as the following optimization problem:

$$\begin{aligned} &\min \frac{1}{2}\|\omega\|^2 + c_l \sum_{i=1}^{l} \xi_i + c_u \sum_{i=l+1}^{m} \xi_i \\ &s.t.\ y_i(\omega^T x_i + b) \geq 1 - \xi_i, \quad i = 1, 2, \ldots, l, \\ &\quad \hat{y}\left(\omega^T x_i + \mathrm{b}\right) \geq 1 - \xi_i, \quad i = l+1, 1+2, \ldots, m, \\ &\quad \xi_i \geq 0, \quad i = 1, 2, \ldots, m, \end{aligned} \tag{1}$$

where $(\omega, b)$ defines a hyperplane; $c_l$ and $c_u$ are user-specified parameters that are used to penalize misclassified samples; $c_u$ is called the "effect factor" of the unlabeled examples in the training process; and $c_u\xi_i$ is called the "effect term" of the unlabeled example in the objective function. The training process of TSVM involves solving the optimization problem that is presented above. The algorithm is as follows:

### C. PARTICLE SWARM OPTIMIZATION ALGORITHM

The basic strategy of particle swarm optimization (PSO) is to initialize the system to a set of random solutions and search for optimal values via iteration. In each iteration, calculate and update the current velocity and position of the particle via the following equation:

$$\begin{cases} V_{id}^{k+1} = \omega V_{id}^{k} + c_1 r_1 (P_{id}^{k} - X_{id}^{k}) + c_2 r_2 (P_{gd}^{k} - X_{gd}^{k}) \\ X_{id}^{k+1} = X_{id}^{k} + V_{id}^{k+1} \end{cases} \tag{2}$$

where $X_i$ is the particle set, $V_i$ is the speed, $c_1$ and $c_2$ are positive constants, $P_i = (P_{i1}, \ldots, P_{id})$ is a locally optimal solution, and $P_g = (P_{g1}, \ldots, P_{gd})$ is a globally optimal solution.

## III. METHOD

### A. FRAMEWORK

This study proposes an AMPSO-SVM-based method for information extraction from high-spatial-resolution multi-spectral remote-sensing images. As illustrated in Fig. 3, this model is mainly composed of the following five steps: 1) pre-processing of the remote-sensing image data; 2) extraction of the spectral information of 4 bands, NDWI values and texture feature to form the objects' feature space that marked within dotted box; 3) division of the data sets to be classified into labeled and unlabeled samples; 4) initialization of the SVM classifier and parameter tuning via the AMPSO algorithm; and 5) output of the results (waterline boundaries and vector diagram).

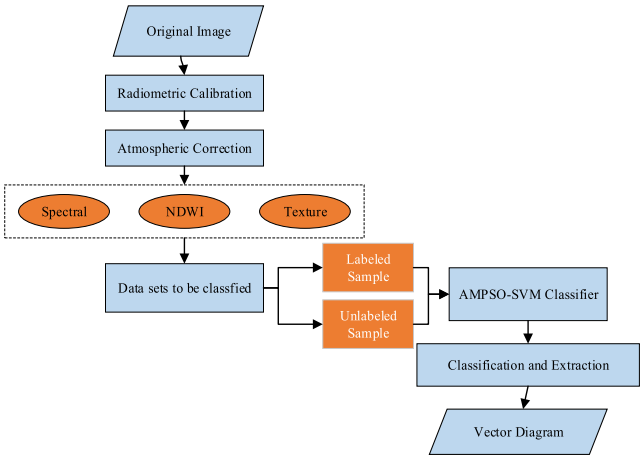


**FIGURE 3.** Framework of the proposed method.

### B. AMPSO-SVM ALGORITHM

According to the model, the relative merits of the method depend on the AMPSO-SVM classifier, which depends on the parameters of SVM. In this part, we analyze and explain why this approach performs better. Machine-learning-based methods utilize a parameter tuning process. Hence, searching for the optimal solution of the algorithm is the main problem on which we focus. However, the input data may be mapped into a high-dimensional space via a nonlinear mapping that spreads the distribution of the data points in a way that facilitates the fitting of a linear hyperplane. On the basis of SVM theory, which is discussed above, in this case, the hyperplane can be computed by using a positive-definite kernel function $k(x, x_i)$, which leads to the following decision function:

$$f(x) = \mathrm{sgn}(\sum_{i=1}^{n} a_i y_i k(x, x_i) + b) \tag{3}$$

where $a_i$ is the Lagrange multiplier. To train the classifier, only the kernel is required; no explicit knowledge is necessary. The identification of the optimal parameter values for SVM is the key problem.

At present, using an intelligent algorithm to optimize the SVM parameter values is the most advanced and effective method. Genetic algorithm and particle swarm optimization are adopted frequently.

PSO has a simple structure and converges fast but always suffers from premature convergence and low iteration efficiency. Therefore, the mutation strategy in genetic algorithm is incorporated into PSO. The convergence state of the particle swarm mainly depends on the fitness function and the characteristics of the problem. All particles having the same position are equivalent to all particles having the same fitness. Then, the overall fitness of all particles is calculated. To describe the state of the particle swarm quantitatively, the colony fitness variance and particle convergence will be defined. A flowchart of the AMPSO-SVM algorithm is shown in Fig. 4.

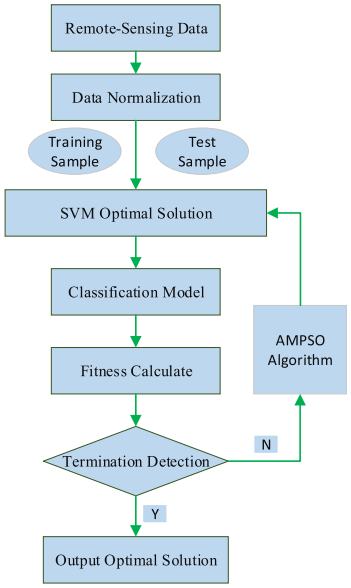


**FIGURE 4.** AMPSO-SVM flowchart.

*Definition 1 Colony fitness variance:* $\sigma^2 = \sum_{i=1}^{n} \left[\frac{f_i - f_{avg}}{f}\right]^2$, where $n$ is the number of particles, $f_i$ is the fitness, $f_{avg}$ is the average fitness, and $f$ is the normalization scaling factor, which is calculated via the following formula:

$$f = \begin{cases} \max\left\{\left|f_i - f_{avg}\right|\right\}, & \max\left\{\left|f_i - f_{avg}\right|\right\} > 1 \\ 1, & others \end{cases} \tag{4}$$

According to this definition, the colony fitness variance reflects the convergence degree of all particles in the particle swarm. The smaller $\sigma^2$ is, the closer the swarm is to converging; if it is large, the swarm is in the random search stage.

*Definition 2 Particle convergence:* $\lim_{t \to \infty} x(t) = p$, where $p$ is a position in space. Hence, the particle will stop at a position eventually.

**TABLE 1.** GaoFen-1 satellite parameters.

| Parameter | 2-m/8-m-resolution multispectral camera | | 16-m-resolution multispectral camera |
|---|---|---|---|
| Spectral Range | Panchromatic | 0.45-0.90 $\mu m$ | |
| | Multispectral | 0.45-0.89 $\mu m$ | 0.45-0.89 $\mu m$ |
| Spatial Resolution | Panchromatic | 2 m | 16 m |
| | Multispectral | 8 m | |
| Width | 60 km (2 cameras) | | 80 km (4 cameras) |
| Return Time | 41 days | | 4 days |

When premature convergence or overall convergence occurs, $\sigma^2$ approaches zero and the particles gather at one or more positions. For all particles, the final convergence position will be the globally optimal value that is found by the whole particle swarm. If the position is unique, all the particles will be there; if other positions exist, the particles will also gather at these positions. The position that is found by the particle swarm may not be the global optimum. Therefore, it is impossible to distinguish premature convergence from global convergence because the variance of the population fitness is zero; it is necessary to further judge whether the optimal solution that has been obtained by the algorithm is the theoretical globally optimal solution.

According to equation (3), the next position of a particle is determined by the current position and speed $V_i$, which depends on the initial speed, $P_{id}$ and $P_{gd}$. If premature convergence has occurred, $P_{gd}$ is a locally optimal solution. Changing $P_{gd}$ will lead to the transformation of the search direction and other areas of the space will be searched. This is repeated until the globally optimal solution has been obtained. Suppose that a better position will be found under $P_{gd}$. The mutation operation is performed by a random operator on $P_{gd}$ with probability $P_m$:

$$P_m = \begin{cases} k, & \sigma^2 < \sigma^2 \; and \; f(P_{gd}) < f_d \\ 0, & others \end{cases} \tag{5}$$

where $f_d$ is the theoretical optimum and $k$ is a random number (in the range [0.1, 0.3]). The mutation operation is realized by adding a random disturbance: $P_{gd}^k = P_{gd}^k(1 + 0.5\eta)$, where $\eta$ obeys a (0,1) Gaussian distribution. This operation continuously shrinks the search space throughout the iterations while maintaining the diversity. According to the algorithm, we measure the classification accuracy under cross-validation via the following fitness function:

$$f = \frac{cc}{cc + uc} \times 100\% \tag{6}$$

where $cc$ denotes the number of correctly classified samples and $uc$ denotes the number of incorrectly classified samples. The algorithm is presented in detail as follows.

**Algorithm 1** 1 TSVM

Input: $D_l$, $D_u$, $C_l$, $C_u$
Training $SVM_l$ with $D_l$
Predict $D_u$, obtain $\hat{y}$
Initialize $C_u \ll C_l$
**While** $C_u < C_l$ do
  Compute $(\omega, b)$ and $\xi$ via equation (1)
  **While** $\exists \{i, j \,|(y_i y_j < 0) \wedge (\xi_i < 0) \wedge (\xi_j < 0) \wedge (\xi_i + \xi_j > 2)\}$
  do $y_i = -y_i$, $y_j = -y_j$
   Compute $(\omega, b)$, $\xi$
  **End while**
   $C_u = \min\{2C_u, C_l\}$
**End while**
Output unlabeled example prediction results $\hat{y}$

**Algorithm 2** AMPSO-SVM

Input: SVM parameters $(c, \gamma)$
Initialize the particle position $(c, \gamma)$
Set $P_b$ and $P_g$
**Do** update $V_i$ and $P_i$
  Calculate $\sigma^2, f\left(P_g\right), P_m$
    If Generate $r \in [0, 1]$ and $r < P_m$
    Then, do $P_{gd}^k$
**while** $\sigma^2 = \sum_{i=1}^{n} \left[\frac{f_i - f_{avg}}{f}\right]^2 = 0$ and $f\left(P_g\right) \geq f_d$
Then, output $P_g$, $(c, \gamma)$

**TABLE 2.** Experimental parameter settings.

| Parameter | Value |
|---|---|
| Population size | 30 |
| Maximum number of iterations | 100 |
| Learning factor | 1.5 |
| KNN number of neighbors | 7 |

## IV. EXPERIMENTAL RESULTS AND ANALYSIS

### A. GAOFEN-1 SATELLITE PARAMETERS

The experiments data is from GaoFen-1 satellite which is equipped with two multispectral scanners with a 2-m-resolution panchromatic band, four 8-m-resolution multi-spectral bands with a two-camera stitching swath width of 60 km, and four 16-m-resolution multispectral bands with a four-camera stitching swath width of 800 km.

According to Table 2, a 16-m-spatial-resolution multispectral remote-sensing image can be obtained in 4 days. Quick image acquisition is helpful for dynamic and timely supervision; therefore, it is more meaningful to study such images. In this article, we select image data that have a spatial resolution of 16 m.

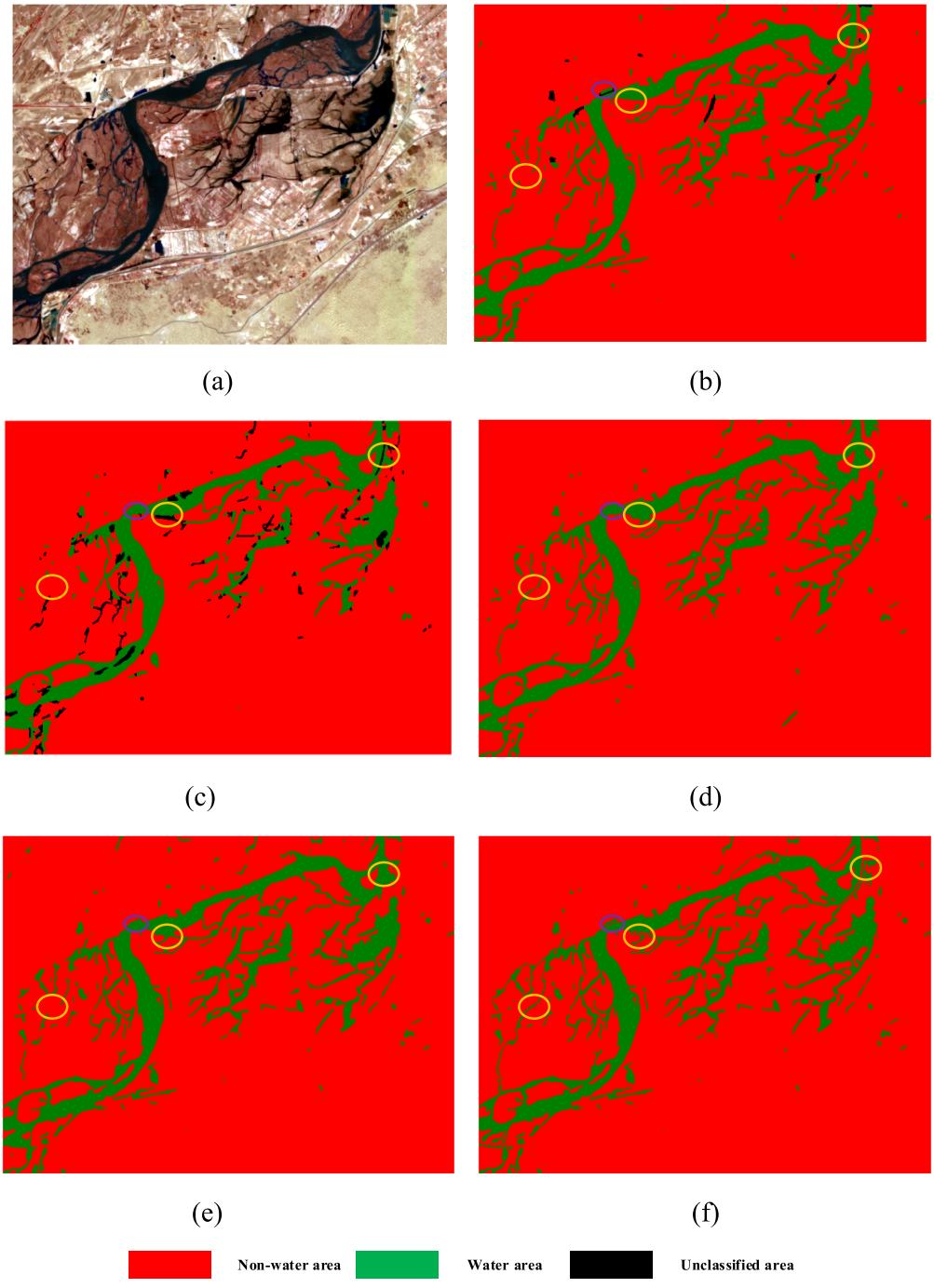


**FIGURE 5.** Study area 1. (a) GF-1 multispectral imagery (a section of the Yellow River, with an area of 711∗531 pixels), (b) extraction result of the KNN method, (c) extraction result of the PCA method, (d) extraction result of the basic SVM method, (e) extraction result of the PSO-SVM method, and (f) extraction result of the AMPSO-SVM method. The green area is the water area, while the red area represents the non-water area.

### *B. EXPERIMENTAL SETTINGS*

In order to evaluate the performance of proposed method, the experiments are conducted on GaoFen-1 remote-sensing images. The region of interest includes rural areas, vegetation, mountains and river, as shown in Fig. 5(a) and Fig. 6(a). This paper presents focuses on river extraction from high-spatial-resolution multispectral remote-sensing images. The preprocessing was realized by ENVI 5.3 and the AMPSO-SVM algorithm was implemented using LibSVM [38] in Python 3.5. As discussed above, in this paper, 6 features were extracted to form the feature space: the spectral indices of band 1, band 2, band 3, and band 4; NDWI;

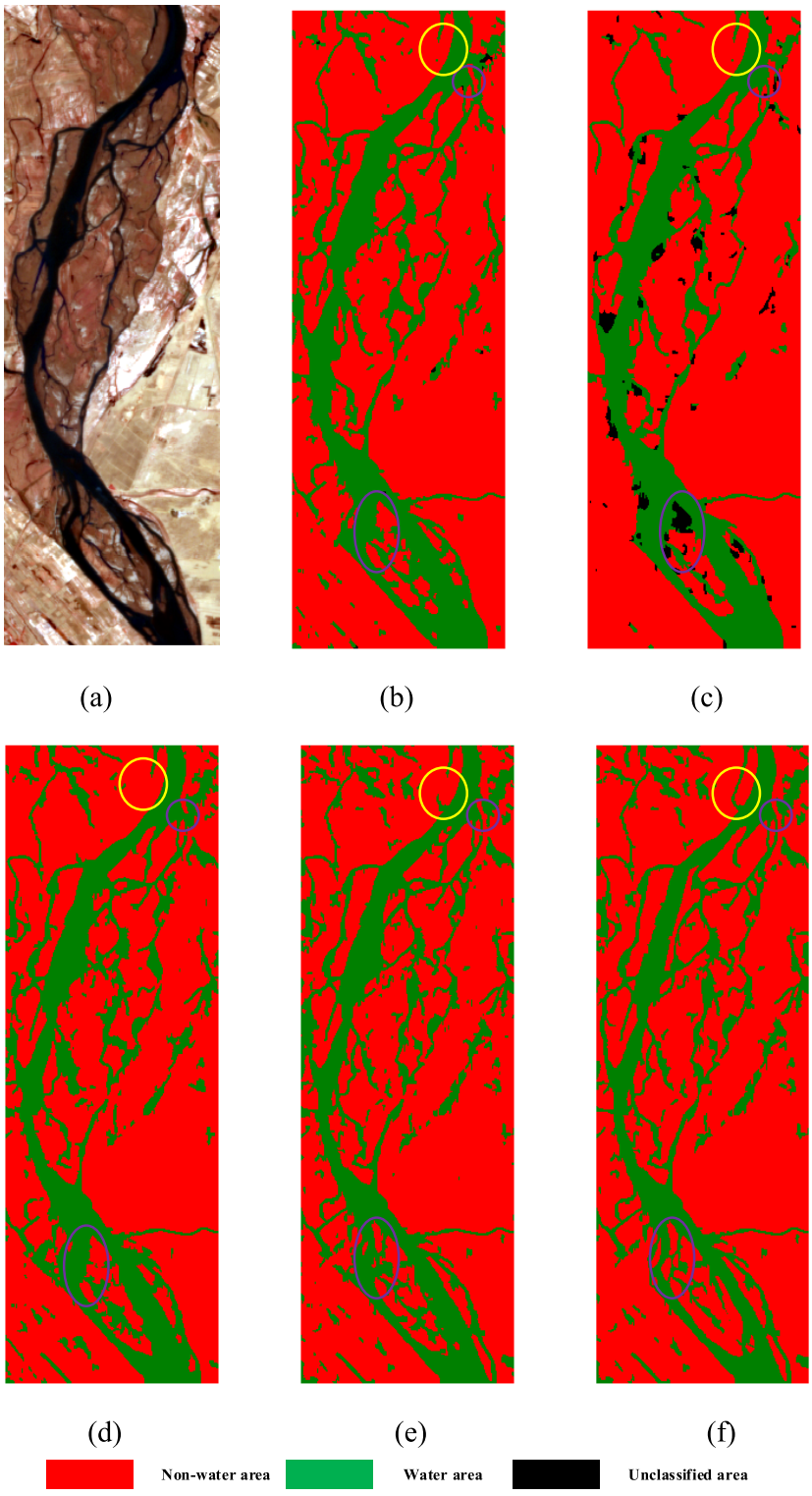


**FIGURE 6.** Study area 2. (a) GF-1 multispectral imagery, (b) extraction result of the KNN method, (c) extraction result of the PCA method, (d) extraction result of the basic SVM method, (e) extraction result of the PSO-SVM method, and (f) extraction result of the AMPSO-SVM method.

and the texture entropy. The test sample is independent from the training data. Our results and analysis will be followed by a comparison with principal component analysis (PCA) and K-nearest neighbor (KNN). To preserve the original spectral features of the ground-truth object, no digital enhancement processing was performed prior to the experiments.

**TABLE 3.** Numbers of training and test samples for 4 categories.

| Category | Label | Training samples | Test samples | Total number |
|---|---|---|---|---|
| farmland | not water | 371 | 550 | 921 |
| forest | not water | 328 | 642 | 970 |
| water | water | 417 | 593 | 1010 |
| other | not water | 364 | 682 | 1046 |
| total number | / | 1480 | 2467 | 3947 |

**TABLE 4.** Accuracy comparison.

| Method | Area | KNN | PCA | SVM | PSO-SVM | AMPSO-SVM |
|---|---|---|---|---|---|---|
| PA | Area 1 | 92.13% | 91.76% | 94.86% | 95.16% | 96.82% |
| | Area 2 | 90.51% | 91.45% | 92.97% | 93.78% | 94.21% |
| UA | Area 1 | 96.63% | 94.12% | 96.86% | 97.16% | 98.19% |
| | Area 2 | 94.13% | 89.72% | 96.58% | 95.01% | 96.33% |
| OA | Area 1 | 91.90% | 91.24% | 92.17% | 92.80% | 94.55% |
| | Area 2 | 91.80% | 90.33% | 91.93% | 94.18% | 94.87% |
| Kappa | Area 1 | 0.8762 | 0.8645 | 0.8811 | 0.8923 | 0.8993 |
| | Area 2 | 0.8631 | 0.8356 | 0.8658 | 0.9079 | 0.9135 |

The parameter settings for the experiment are listed in Table 2. The initial positions of particles were produces as positive a value and their associated velocities could be a positive or negative value. We initialized 30 as the population size based on the extent of searching area. The maximum number of iterations ensure that the convergence is achieved within the number of iterations, and this value helps us analyze the iteration efficiency. Small learning factor leads to inefficient learning and big value leads to overfitting. Therefore we choose 1.5 as the learning factor in our experiments.

Prior to evaluating the classification results, we randomly select a subdomain for training and testing the SVM classifier. The number of training and test samples from the images are listed in Table 3.

### C. COMPARISON IN TERMS OF ACCURACY

As discussed previously, the main objective of the study was to extract river bodies accurately. The proposed method has an advantage in river delineation. As shown in Fig. 5(a) and Fig. 6(a), which are referred to as area 1 and area 2, the image contains a section of the Yellow River. It was captured by the GaoFen-1 satellite. Area 1 covers river, reservoir and a narrow water body with an area of 711∗531 pixels, while area 2 primarily covers river with substantial rocky reef and between mountains with an area of 187∗555 pixels. The accuracy is evaluated in terms of PA (Producer Accuracy), UA (User Accuracy), OA (overall accuracy) and the kappa coefficient relative to the ground-truth map via a confusion matrix, which is calculated according to the position of each pixel and the classification of the corresponding image.

The accuracy comparison is presented in Table 4. Under the same scenario, SVM-based methods yield higher overall accuracy than other object-based methods in the two study areas and the kappa coefficients are similar. Besides, the PA (Producer Accuracy) and UA (User Accuracy) performs same trend. The classified results have a high consistency according to a random sample. Moreover, the SVM-based methods always get better PA and UA than KNN and PCA method. This gives rise from the advantages of SVM in classification with limit information. An average increase in accuracy of nearly 2 percent is realized by SVM-based methods, according to the results. For the SVM-based methods, the extraction results differ among the parameter tuning methods because the selection of the final parameter values is directly related to the accuracy of the machine learning classifier. The AMPSO-SVM method can yield 94.5% accuracy in area 1 and area 2, which is higher compared to other methods, with a similar kappa coefficient. The improvements in the accuracy and kappa coefficient of the extraction result are substantial.

According to a visual inspection, AMPSO-SVM successfully extracted most of the river water body, including narrow tributary water body information, in study areas 1 and 2. Based on the feature space of the objects that we discussed above, the KNN, PCA, and SVM-based methods ignore the mountain shadow interference. This demonstrates the superior feature space construction performance of the proposed method. By considering both the texture and spectral features, the object-based methods substantially outperform the existing object feature space construction methods. According to Fig. 5 and Fig. 6, the SVM-based extraction methods

**TABLE 5.** Parameter comparison.

| Classification model | Penalty parameter | Kernel function parameter | Overall accuracy | Kappa |
|---|---|---|---|---|
| Basic SVM | 100 | 0.143 | 92.05% | 0.8734 |
| PSO-SVM | 166.9423 | 1.366 | 93.13% | 0.8891 |
| AMPSO-SVM | 246.7891 | 0.134 | 94.29% | 0.9061 |

outperformed PCA and KNN and objects are omitted in the PCA and KNN extract results. SVM-based methods yield satisfactory generalization performance and have strong robustness in the case of small-sample data. The area that is surrounded by a purple circle in Fig. 5 and Fig. 6 is classified differently by the methods; according to the ground truth, only AMPSO-SVM could precisely distinguish it. For the spot that is surrounded by yellow circle in Fig. 5, the result specifies the clear river boundaries against the river inland, which has lower reflectance.

For the wide river areas, there was little difference among the methods. This is because of the advantages of object-based method and the use of the same feature space. Meanwhile, the NDWI was adopted as one of the spectral features, which helps increase the discrimination between the river water body and other noise. A significant difference is observed in the purple circles in Fig. 5 and Fig. 6: The AMPSO-SVM outperforms PSO-SVM in terms of the continuity and consistency of the water body, as indicated by the yellow circles in Fig. 6(e) and Fig. 6(f). Because the parameters in AMPSO-SVM are both local and global optimal solutions, the local details and global accuracy are relatively improved compared with PSO-SVM and basic SVM.

In summary, according to the results of the experiments, the feature space and the classification method are the core factors that determine the accuracy of the final result. First, we select spectral bands, NDWI, and texture entropy to form the feature space; this approach substantially outperforms the existing feature selection method. Second, the SVM-based method is useful in the research fields of remote-sensing image classification and extraction. Third, the optimization of SVM could further improve the performance of the classifier and lead to better results and the superior performance of AMPSO has been demonstrated.

### D. SELECTION OF PARAMETERS

During the extraction process, PSO-SVM and AMPSO-SVM differ substantially in terms of the speed and efficiency of parameter optimization. In Fig. 7, the two curves have noticeably differences: AMPSO-SVM always converges after approximately 6 iterations, while the PSO-SVM algorithm requires more than 10 iterations. Moreover, the AMPSO-SVM algorithm yields a higher final fitness than PSO-SVM after dozens of iterations. The fitness represents the degree of the classification accuracy. When convergence has been realized, the classification accuracy tends toward the optimal value. The faster convergence of the proposed method is due to the mutation operator, which enables PSO-SVM to escape from a local extremum as quickly as possible, which results in superior performance of the PSO-SVM algorithm.

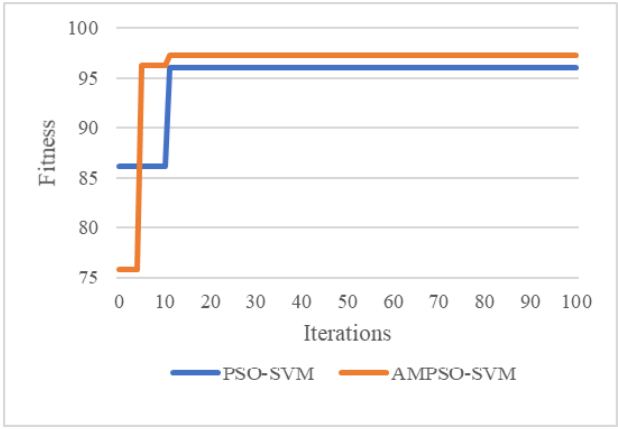


**FIGURE 7.** Iteration efficiency.

The AMPSO algorithm compares the colony fitness variance with the globally optimal solution to judge whether it has fallen into a local extremum and the mutation operator enables it to escape from of local extrema quickly. AMPSO-SVM overcomes the subjectivity of the PSO-SVM algorithm and escapes from local extrema quickly. The final parameters that obtained based on local extrema always have low fitness, which are not the optimal parameters in whole images. The iterations represents the optimal parameters are obtained. In means the less iterations equals the better performance.

The parameter selection results are listed in Table 5. Compare with the basic SVM and PSO-SVM algorithms, the AMPSO-SVM's parameter values yield the highest overall accuracy because the introduction of the mutation operator into PSO optimizes the processing, which leads to optimal parameters that directly increase the classification accuracy.

## V. CONCLUSION

This paper analyzed the shortcomings of the existing river extraction methods, such as the water index, PCA, KNN, and basic SVM, for high-spatial-resolution remote-sensing images and proposed an improved SVM algorithm that considers the correlation between the spectral and spatial characteristics to distinguish the river water pixels. During the process, better parameter values lead to more accurate results. Therefore, we improved the process of SVM parameter optimization by incorporating the mutation particle swarm optimization algorithm, which adds the mutation operator

into the PSO algorithm. Compared with PCA, KNN, basic SVM and the PSO-SVM method, the proposed method yields higher overall accuracy on the Yellow River image from the GaoFen-1 satellite. According to the confusion matrix, the kappa coefficient demonstrates similar performance. It is demonstrated that the proposed method accurately delineates the river bodies, including the relatively narrow water body, and effectively ignores the interference of background noise, such as mountain shadows.

The proposed approach is suitable for extracting river information from GaoFen-1 remote-sensing images. It is useful for monitoring rivers to ensure water safety, such as for flood warning, via river area extraction. According to this study, the machine-learning-based method is superior to the traditional method. The most advanced research direction is to use a hybrid approach of computer science and machine learning. Further study is expected to follow two directions: further optimization of the performance of the SVM optimal parameter selection method and investigation of the application of similar approaches to river extraction, such as random forests and neural networks.

## REFERENCES

[1] A. Harrison *et al.*, "The regional and global significance of nitrogen removal in lakes and reservoirs," *Biogeochemistry*, vol. 93, nos. 1–2, pp. 143–157, 2009.
[2] J. Trancik *et al.*, "Lakes and reservoirs as regulators of carbon cycling and climate," *Limnol. Oceanogr.*, vol. 54, no. 6, pp. 2289–2314, 2009.
[3] T. D. Fletcher, H. Andrieu, and P. Hamel, "Understanding, management and modelling of urban hydrology and its consequences for receiving waters: A state of the art," *Adv. Water Resour.*, vol. 51, pp. 279–2013, Jan. 2013.
[4] S. Stendera *et al.*, "Drivers and stressors of freshwater biodiversity patterns across different ecosystems and scales: A review," *Hydrobiologia*, vol. 696, no. 1, pp. 1–28, 2012.
[5] L. Carvalho *et al.*, "Sustaining recreational quality of European lakes: Minimizing the health risks from algal blooms through phosphorus control," *J. Appl. Ecol.*, vol. 50, no. 2, pp. 315–323, 2013.
[6] P. Rizzo, "Water and wastewater pipe nondestructive evaluation and health monitoring: A review," *Adv. Civil Eng.*, vol. 2010, May 2010, Art. no. 818597.
[7] Y. Byun, Y. Han, and T. Chae, "Image fusion-based change detection for flood extent extraction using bi-temporal very high-resolution satellite images," *Remote Sens.*, vol. 7, no. 8, pp. 10347–10363, 2015.
[8] X. Yang, S. Zhao, X. Qin, N. Zhao, and L. Liang, "Mapping of urban surface water bodies from sentinel-2 MSI imagery at 10 m resolution via NDWI-based image sharpening," *Remote Sens.*, vol. 9, no. 6, p. 596, 2017.
[9] National Research Council, *Integrating Multiscale Observations of U.S. Waters*. Washington, DC, USA: National Academies Press, 2008, pp. 16–64.
[10] S. R. Proud, R. Fensholt, L. V. Rasmussen, and I. Sandholt, "Rapid response flood detection using the MSG geostationary satellite," *Int. J. Appl. Earth Observ. Geoinf.*, vol. 13, no. 4, pp. 536–544, 2011.
[11] S. D. Jawak, K. Kulkarni, and A. J. Luis, "A review on extraction of lakes from remotely sensed optical satellite data with a special focus on cryospheric lakes," *Adv. Remote Sens.*, vol. 4, pp. 196–213, Sep. 2015.
[12] H. Xu, "Modification of normalised difference water index (NDWI) to enhance open water features in remotely sensed imagery," *Int. J. Remote Sens.*, vol. 27, no. 14, pp. 3025–3033, 2006.
[13] G. L. Feyisa, H. Meilby, R. Fensholt, and S. R. Proud, "Automated Water Extraction Index: A new technique for surface water mapping using Landsat imagery," *Remote Sens. Environ.*, vol. 140, pp. 23–35, Jan. 2014.
[14] L. Cheng, J. Gong, X. Yang, C. Fan, and P. Han, "Robust affine invariant feature extraction for image matching," *IEEE Geosci. Remote Sens. Lett.*, vol. 5, no. 2, pp. 246–250, Apr. 2008.
[15] H. Sebai, A. Kourgli, and A. Serir, "Dual-tree complex wavelet transform applied on color descriptors for remote-sensed images retrieval," *Proc. SPIE*, vol. 9, no. 1, pp. 95917–95994, 2015.
[16] F. Xu, "Segmentation of remote sensing imagery based on Gabor texture description," *Sci. Surveying Mapping*, vol. 38, no. 1, pp. 116–124, 2013.
[17] Y. Yang, W. Wan, S. Huang, F. Yuan, S. Yang, and Y. Que, "Remote sensing image fusion based on adaptive IHS and multiscale guided filter," *IEEE Access*, vol. 4, pp. 4573–4582, 2016.
[18] P. Shao, G. Yang, X. Niu, X. Zhang, F. Zhan, and T. Tang, "Information extraction of high-resolution remotely sensed image based on multiresolution segmentation," *Sustainability*, vol. 6, no. 8, pp. 5300–5310, 2014.
[19] G. Castilla, "Size-constrained region merging: A new tool to derive basic landcover units from remote sensing imagery," in *Proc. ESA-EUSC-Theory Appl. Knowl.-Driven Image Inf. Mining Focus Earth Observ.*, Madrid, Spain, 2004, pp. 1–9.
[20] C. William *et al.*, *Object-Based Image Analysis: Spatial Concepts for Knowledge-Driven Remote Sensing Applications* (Lecture Notes in Geoinformation and Cartography). Berlin, Germany, 2008, pp. 2–11.
[21] Z. Ganim and A. Tokmakoff, "Spectral signatures of heterogeneous protein ensembles revealed by MD simulations of 2DIR spectra," *Biophys. J.*, vol. 91, no. 7, pp. 2636–2646, 2006.
[22] B. Li, H. Zhang, and F. Xu, "Water Extraction in high resolution remote sensing image based on hierarchical spectrum and shape features," *IOP Conf. Ser., Earth Environ. Sci.*, vol. 17, no. 1, 2014, Art. no. 12123.
[23] D. Chabot, C. Dillon, A. Shemrock, N. Weissflog, and E. P. S. Sager, "An object-based image analysis workflow for monitoring shallow-water aquatic vegetation in multispectral drone imagery," *ISPRS Int. J. GeoInf.*, vol. 7, no. 8, p. 294, 2018.
[24] N. Selmes, T. Murray, and T. D. James, "Fast draining lakes on the Greenland Ice Sheet," *Geophys. Res. Lett.*, vol. 38, no. 15, pp. 165–176, 2011.
[25] M. Belgiu and L. Dragut, "Comparing supervised and unsupervised multiresolution segmentation approaches for extracting buildings from very high resolution imagery," *ISPRS J. Photogramm. Remote Sens.*, vol. 96, pp. 67–75, Oct. 2014.
[26] D. Li, G. Zhang, Z. Wu, and L. Yi, "An edge embedded marker-based watershed algorithm for high spatial resolution remote sensing image segmentation," *IEEE Trans. Image Process.*, vol. 19, no. 10, pp. 2781–2787, Oct. 2010.
[27] Y. Zhang, "A method for continuous extraction of multispectrally classified urban rivers," *Photogramm. Eng. Remote Sens.*, vol. 66, no. 8, pp. 991–999, 2000.
[28] Z. F. Shen, L. G. Xia, and J. L. Li, "Automatic and high-precision extraction of rivers from remotely sensed images with Gaussian normalized water index," *J. Image Graph.*, vol. 18, no. 4, pp. 421–428, 2013.
[29] G. M. Foody and A. Mathur, "A relative evaluation of multiclass image classification by support vector machines," *IEEE Trans. Geosci. Remote Sens.*, vol. 42, no. 6, pp. 1335–1343, Jun. 2004.
[30] H. Azizi, E. Akbari, and N. Amiri, "Remote sensing and land use extraction for kernel functions analysis by support vector machines with ASTER multispectral imagery," *Iranian J. Earth Sci.*, vol. 4, no. 2, pp. 75–84, 2012.
[31] J. Chen, C. Wang, and R. Wang, "Using stacked generalization to combine SVMs in magnitude and shape feature spaces for classification of hyperspectral data," *IEEE Trans. Geosci. Remote Sens.*, vol. 47, no. 7, pp. 2193–2205, Jul. 2009.
[32] Y. Guo, X. Jia, and D. Paull, "Effective sequential classifier training for SVM-based multitemporal remote sensing image classification," *IEEE Trans. Image Process.*. vol. 27, no. 6, pp. 3036–3048, Jun. 2018.
[33] Y. Liu, B. Zhang, L. Huang, and L. Wang, "A novel optimization parameters of support vector machines model for the land use/cover classification," *J. Food Agricult. Environ.*, vol. 10, no. 2, pp. 1098–1104, 2012.
[34] Q. Zhang *et al.*, "A novel method for urban area extraction from VIIRS DNB and MODIS NDVI data: A case study of Chinese cities," *Int. J. Remote Sens.*, vol. 38, no. 21, pp. 6094–6109, 2017.
[35] J. Li, "A novel remote sensing image classification algorithm based on PCA and hidden Markov random field theory," in *Proc. Online Int. Conf. Green Eng. Technol.*, 2016, pp. 1–5.
[36] G. Alimjan, T. Sun, H. Jumahun, Y. Guan, W. Zhou, and H. Sun, "A hybrid classification approach based on support vector machine and k-nearest neighbor for remote sensing data," *Int. J. Pattern Recognit. Artif. Intell.*, vol. 31, no. 10, pp. 12585–12591, 2017.
[37] M. Pal and P. M. Mather, "Support vector machines for classification in remote sensing," *Int. J. Remote Sens.*, vol. 26, no. 5, pp. 1007–1011, 2005.
[38] C. C. Chang and C. J. Lin, "LIBSVM: A library for support vector machines," *ACM Trans. Intell. Syst. Technol.*, vol. 2, no. 3, pp. 1–27, 2011.

**XIN LI** (M'08) received the B.S. degree from Zhengzhou University and the M.S. degree from Hohai University, Nanjing, China, where he is currently pursuing the Ph.D. degree in computer science and technology with the College of Computer and Information. His research interests include computer vision and remote sensing image processing.

**XIN LYU** is currently a Lecturer with the College of Computer and Information, Hohai University. His research interests include cryptography, network information security, and privacy-preserving theory and technology. He has published more than 20 papers in refereed international journals and conference proceedings.

**YAO TONG** received the B.S. and M.S. degrees from Hohai University. She is currently pursuing the Ph.D. degree in software engineering with the Industrial Technology Research Institute, Zhengzhou University, Zhengzhou, China. Her research interests include artificial intelligence and service computing.

**SHENGYANG LI** received the Ph.D. degree in hydrographic remote sense from Delft University. He is currently a Professor of engineering with the Yellow River Conservancy Commission. He had more than 20 years of industry working and management experience on water conservancy project and remote sensing technology. He has published more than 20 publications in international journals and conferences. He has participated in the completion of key technologies for remote sensing monitoring of water resources in the Yellow River and formulated many industry standards.

**DAOFANG LIU** received the M.S. degree in human geography. He is currently a Senior Engineer with Yellow River Conservancy Commission. He has published more than ten papers in his research field. He was involved in the application of remote sensing technology for 18 years, participated in many remote sensing monitoring projects of flood control, ice control, and soil and water conservation of the Yellow River.